IEEE Access
Multidisciplinary | Rapid Review | Open Access Journal

Received July 28, 2020, accepted August 14, 2020, date of publication August 18, 2020, date of current version August 31, 2020.

Digital Object Identifier 10.1109/ACCESS.2020.3017662

Posture Control of a Four-Wheel-Legged Robot With a Suspension System

LIWEI NI, FANGWU MA, AND LIANG WU
State Key Laboratory of Automotive Simulation and Control, Jilin University, Changchun 130012, China
College of Automotive Engineering, Jilin University, Changchun 130012, China

Corresponding author: Liang Wu (astdwxg@jlu.edu.cn)

This work was supported in part by the National Natural Science Foundation of China under Grant 51705185, in part by the Science and Technology Development Plan of Jilin Province under Grant 20190103056JH, and in part by the National Key Technologies Research and Development Program of China during the 13th Five-Year Plan Period under Grant 2017YFC0601604.

ABSTRACT To achieve posture control and ride comfort (vibration isolation performance) of a robot in unstructured terrain, a novel four-wheel-legged robot (FWLR) with an actively-passively suspension system is first designed. In the suspension system, the active parts are responsible for posture control and the passive parts are responsible for vibration isolation. Then, a closed-loop and decoupled posture control model with 11 DOF are proposed, with which we designed the posture controller with a second-order low-pass filter (SLPF). To test the posture control performance of FWLR in unstructured terrain, both simulation and experiment are carried out, the simulation and experimental results show that the posture angles in unstructured terrain are reduced by 54.65% and 59% on average, respectively. In addition, the frequency response shows that the posture angles are reduced by more than 50% in low-frequency unstructured terrain. Finally, to validate the ride comfort of FWLR, dynamic models with different degrees of freedom (DOF) are established and simulated, and the results present that the ride comfort can be improved with the posture angular acceleration is reduced by 15.83% and 46.7% on average. Generally, with the actively-passively suspension system proposed in this article, FWLR can be equipped with excellent ride comfort and posture control in unstructured terrain. The research in this article has potential reference value and practical value for enriching the posture control of robots and vehicles.

INDEX TERMS Wheel-legged robot, dynamic models, posture control, ride comfort.

I. INTRODUCTION

Wheel-legged all-terrain mobile robots (WLATMR) have the advantages of wheeled robots and legged robots [1] and have a wide range of applications in the fields of post-disaster rescue [2], [3], resource exploration [4], [5], precision agriculture [6] and other fields [7], [8]. Furthermore, WLATMR can replace people by working in extreme surroundings and thus reduce the dangers posed to humans. Therefore, posture control and ride comfort in an unstructured environment are two critical requirements of WLATMR [9], [10], and both of them are studied in this article.

There is no doubt that the posture of a robot can be changed in an unstructured terrain, thus, the off-road ability and stability are reduced. Therefore, posture control is a good way to solve these above problems, and the posture control of WLATMR has attracted considerable attention. For example, Ma *et al.* [11] proposed a wheel-legged all terrain mobile robot with active suspension and thus improved the pitch angle in unstructured terrain. Garcia *et al.* [12] described the locomotion control of a leg prototype, designed and developed to make a quadruped walk dynamically while exhibiting compliant interaction with the uneven terrain. Wei *et al.* [13] provided an approach to generate hopping pattern at stance phase and control it. The effectiveness of the proposed model and control scheme is verified through the simulation and experiments. He *et al.* [14] studied dynamics and posture control of a one-legged hopping robot with articulated leg. To ensure the controllability of the elastic underactuated mechanism, a dynamics synthesis method is proposed for designing the underactuated mechanism so that the dynamics of the system can be transformed into the strict feedback normal form. Cordes *et al.* [15] depicted the mechanical design of a rover, to realize posture control,

The associate editor coordinating the review of this manuscript and approving it for publication was Chua Chin Heng Matthew.

kinematic considerations for movement constraints on the wheel contact points are presented. Iagnemma *et al.* [16] developed a novel rover with the ability to reconfigure its structure to improve posture in unstructured terrain. Wettergreen *et al.* [17] proposed a robot called Scarab, which can adjust the wheelbase and height to keep its drill in contact with the ground and can also adjust its posture to better adapt to uneven terrain. Wilcox *et al.* [18] showed a robot called ATHLETE, which is capable of efficient rolling mobility and walking mobility on extreme terrain. Similar studies include the robots Tri-star [19], Workpartner [20], and Mammoth [21].

Although posture control has been studied by many researchers, most of these methods have been tested in the laboratory, and the experimental terrains have been relatively simple. Furthermore, even if the accuracy of the model and algorithm is not high, it can achieve excellent performance, so the posture control of many robots has remained in the open-loop control or coupled state. However, if the robots are in unstructured terrain, the performance will be reduced. Moreover, since most wheel-legged robots have no elastic system, the traditional modelling method is to regard the robot as a multi-rigid-body, but for the robots with elastic elements in their structure, it will lead to huge error. For example, Luo *et al.* [22] depicted a wheel-legged robot with an elastic structure, and the simulation and experimental results showed that the robot achieved posture control and vibration isolation performance in unstructured terrain, but the control accuracy is affected since the elastic element is regarded as a rigid body. Jiang *et al.* [1] proposed a wheel-legged robot that can travel over unstructured terrain based on active posture control and passive spring-damping system, however, the spring-damping system is still regarded as a rigid body when modelling. Grand *et al.* [23], [24] showed a four-wheel-legged robot that has excellent off-road ability, and its posture is well controlled, but the experiment is carried out in moderate terrain. Bazeille *et al.* [25] studied the posture control of HyQ in unstructured terrain. However, its posture control mainly depends on environment perception, and its control accuracy is easily disturbed by the external environment.

Importantly, if the impact force from the terrain is very huge, the posture can be affected and the ride comfort can be reduced, so achieving an excellent ride comfort in unstructured terrain is an another essential requirement for a wheel-legged robot, and the most effective approach is to equip a vibration isolation system [26], [27]. The reasons for equipping robots with a vibration isolation system are as follows:

1) A chatter or bouncing between the tyres and the terrain can occur in the moment of abrupt contacts, causing a temporary loss of contact force.
2) Substantial acceleration from the terrain can damage the weakest mechanical components of the robot (e.g. actuator), especially in extremely unstructured terrain.
3) Impact energy caused by the terrain can be significantly absorbed by equipping with a suspension system, thereby enhancing the ride comfort performance while achieving all-terrain driving.

Generally, it is necessary to equip a vibration isolation system for all-terrain mobile robots, but traditional wheel-legged robots rarely feature vibration isolation system. For example, CDRDA developed a hybrid wheel-legged robot by including hydraulic joints and electric wheels [28], although the hydraulic mechanism can absorb part of the impact force, there is still a huge impact force on the robot in unstructured terrain. Sun *et al.* [29] presented a decoupled control method based on kinematic models of an amphibious reconfigurable robot called eQuad. Therefore, the proposed robot can walk with a unique gait by eliminating the swing phase of each legs, and it has a balanced posture in unstructured terrain because all legs are in contact with the terrain while walking. However, due to the lack of vibration isolation system, the joint force is huge, which limits its application. Nakajima *et al.* [30] proposed a basic control method for a wheel-legged robot moving on unexplored rough terrains. Based on the proposed control algorithm, the posture of the robot is well controlled, but due to the lack of vibration isolation system, the unstructured terrain will have huge impact on the joints and body.

Although few scholars pay attention to the vibration isolation of WLATMR, some researchers had tried to equip elastic components for wheeled robots, legged robots and wheeled vehicles. For example, Xie *et al.* [31] proposed a robust control method for wheeled vehicles with active suspension, the simulation results show that the vertical acceleration, pitch acceleration and roll acceleration are reduced by 23.07%, 13.24% and 19.63%, respectively. Zhu *et al.* [32] used semi-active suspension and fuzzy control method to achieve the posture control of wheeled vehicle. The simulation results show that the roll angle is reduced by approximately 30% and the ride comfort is improved when changing lanes. Zheng *et al.* [33] designed a semi-active suspension for a wheeled vehicle based on MR damper. The posture control is realized by fuzzy control, and the simulation results present that the pitch and roll angles are reduced by approximately 30% and the vibration isolation performance is enhanced under the steering condition. To solve the problems of energy-saving control, non ideal actuator, and actuator fault tolerance, the nonlinear characteristics of active suspension are studied based on finite-time control [34], bio-inspired control [35] and adaptive control [36]. The simulation and experimental results show that the dynamic system performance of the suspension and the ride comfort of the wheeled vehicle are improved.

In addition, Tharakeshwar and Ghosal [37] added a suspension system for a wheeled robot to increase ride comfort performance and stability. Chen *et al.* [38], [39] improved the ride comfort performance of a hexapod robot by adding rubber to the feet, thus realizing gait planning and posture control. Li *et al.* [40] designed a quadruped robot with

LCS (Linkage-Cable-Spring) mechanism, and achieved excellent ride comfort and posture control performance. These studies provide reference for the research of vibration isolation and ride comfort of wheel-legged robots.

Overall, the traditional WLATMR seldom involves vibration isolation system, and the research on ride comfort is seldom considered, In addition, the modeling method of posture control usually regards the robot as a rigid body. These problems limit the development of WLATMR. Based on the above analysis, a wheel-legged robot with suspension system is proposed, and its posture control and ride comfort are studied.

In this article, to solve the problem of posture control and vibration isolation of WLATMR, a four-wheel-legged all terrain mobile robot with actively-passively suspension system called FWLR is proposed. Each leg of FWLR has an independent passive vibration isolation system and active posture control system that does not interfere with each other. The passive system mainly comprises a spring-damping, and the active system is mainly composed of an actuator, both of which are connected in series, as shown in **Fig. 1**. Relying on the passive vibration isolation system, FWLR can continuously keep the tyres in contact with the ground all the time, and absorb the ground impact from the terrain. By relying on the active system, FWLR can reconfigure its posture by actuators. Thus the posture control performance and ride comfort can be effectively improved by the actively-passively suspension system proposed in this article.

In this article, to validate the posture control performance in unstructured terrain, a closed-loop and decoupled posture control model with 11DOF is proposed, with which the LQR posture controller with SLPF is designed. In addition, the terrain estimation model based on a gyroscope is presented. To verify the posture control performance, both simulation and experiment are carried out and compared, the results show that FWLR has good posture control ability. Besides, to validate the ride comfort of FWLR, the dynamic models with different DOF are established and compared, and the results show that the ride comfort can be improved by the actively-passively suspension.

This article is organized as follows. The next section provides the design of the prototype. The posture control is established in Section 3. The ride comfort is completed in Section 4. The conclusions are presented in Section 5.

II. PROTOTYPE DESIGN

A. DESIGN CONCEPT

A good way to improve the performance of a robot in unstructured terrain is to use structure optimization [41], [42], therefore, according to the principle diagram shown in **Figs. 1(a)**, a wheel-legged structure with an actively-passively suspension system is designed in **Figs. 1(b)**, and the real model of the novel wheel-legged is depicted in **Figs. 1(c).** The suspension system is mainly composed of an actuator and a spring-damping, the posture control of FWLR is achieved by four actuators, and the length of the output of the actuator is treated

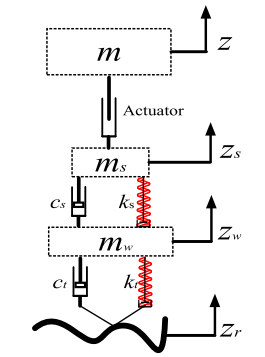

(a) Principle diagram

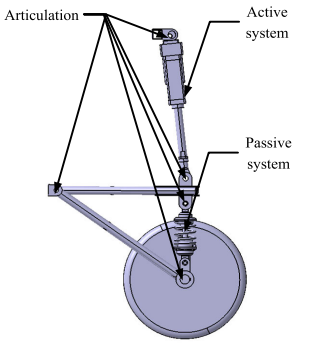

(b) 3D model

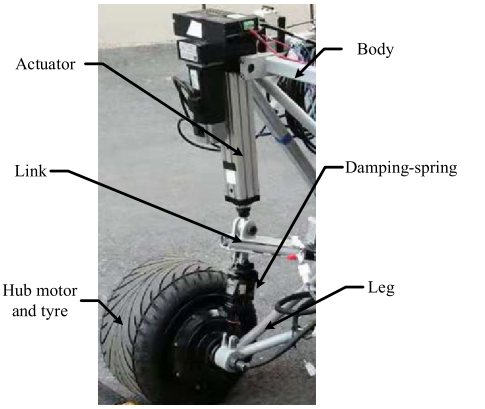

(c) Real model

FIGURE 1. Actively-passively suspension system of FWLR.

as the input of the control system. Moreover, to improve the ride comfort in unstructured terrain, the spring-damping system is connected in series with the actuator, and this design makes it possible for FWLR to have both posture control and ride comfort at the same time. In this article, the posture control is achieved by the active system, and the excellent ride comfort is equipped by the combination of the posture control and the passive system.

B. STRUCTURE PARAMETERS

As illustrated in **Fig. 2,** FWLR consists of the body, battery, controller, actuators, motor drivers, legs, spring-damping, etc. FWLR is a symmetrical structure, and the specific parameters are illustrated in **Tab. 1.** The virtual and real model are shown

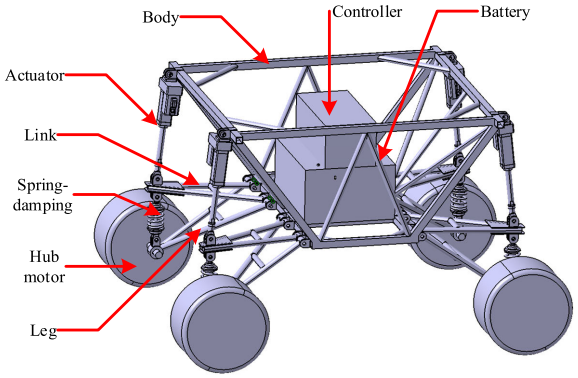

(a) Virtual model

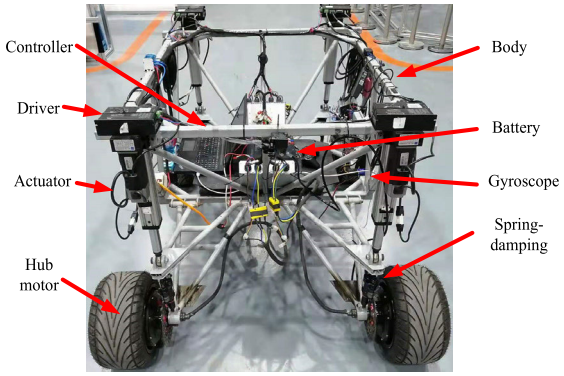

(b) Real model

FIGURE 2. Model of FWLR.

TABLE 1. Main parameters of FWLR.

Parameters	Value
Wheel radius (r)	190 mm
Actuator initial length (l)	480 mm
1/2 wheelbase (a)	651 mm
1/2 wheelbase (b)	600 mm
Centroid height (h)	460 mm
Pitching moment of inertia (I_p)	14.32 $kg{\cdot}m^2$
Rolling moment of inertia (I_r)	15.73 $kg{\cdot}m^2$
Wheel mass (m_{wi})	10 kg
tyre stiffness (k_{ti})	200000 N/m
tyre damping (c_{ti})	50 N·s/m
Body mass (m)	100 kg
Spring stiffness (k_{si})	20000 N/m
Damper damping coefficient (c_{si})	1000 N·s/m

in **Figs. 2(a)** and **2(b)**, respectively, and the balanced posture in unstructured terrain is shown in **Figs. 3(a)** and **3(b)**.

The proposed robot can traverse over unstructured terrains by the actively-passively suspension system proposed in this article. The advantages of the suspension system are shown below:

1) The posture is controlled by four actuators, which ensures the pitch and roll of the robot can be decoupled, thus it is convenient for posture control.

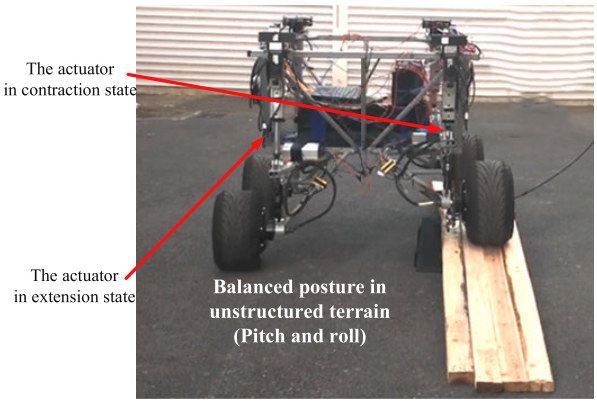

FIGURE 3. Posture control of FWLR.

2) The combination of passive system and active system can achieve the advantages of both approaches, therefore, the ride comfort and posture control performance of the robot in unstructured terrain can be enhanced at the same time.

Overall, this article presents a novel wheel-legged robot with the posture and ride comfort that can be improved according to the terrain.

III. POSTURE CONTROL

A. DYNAMIC MODEL

Compared to traditional robots, the existence of spring-damping system makes the control system more complex, and FWLR can not be regarded as a rigid system. Therefore, an 11 DOF dynamic model considering the suspension system and linear quadratic regulator (LQR) algorithm are built to achieve the posture control in unstructured terrain, and the pitch angle and roll angle are decoupled with closed-loop control. In addition, to fully leverage the advantages of actuators and realize the controllability of the system, two second-order low-pass filters (LPF) in series are established, as shown in **Fig. 4**, Equation. (1-8) describe the dynamic model, among which, Eqs. (6-7) refer to the corresponding filter model. In this section, the roll and pitch angles are used to describe the posture of the robot.

The equation of the vertical motion of the body is given by

$$m\ddot{z} = F_1 + F_2 + F_3 + F_4 \tag{1}$$

The equation of the pitch motion of the body is given by

$$I_P\ddot{\theta} = (F_1 + F_2 - F_3 - F_4)a \tag{2}$$

The equation of the roll motion of the body is given by

$$I_r\ddot{\phi} = (F_1 + F_3 - F_2 - F_4)b \tag{3}$$

The equations of the vertical motion of the links, $i = (1{\sim}4)$ is given by

$$m_{si}\ddot{z}_{si} + F_i = c_{si}(\dot{z}_{wi} - \dot{z}_{si}) + k_{si}(z_{wi} - z_{si}) \tag{4}$$

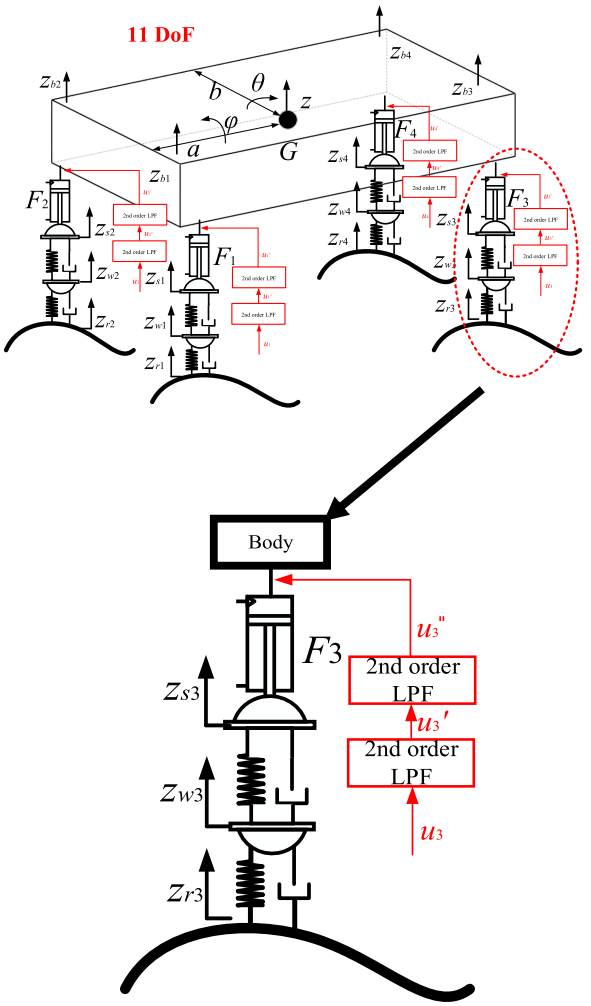

FIGURE 4. Dynamic model with low-pass filter.

The equations of the vertical motion of the tyres, $i = (1\sim4)$ is given by

$$m_{wi}\ddot{z}_{wi} = c_{si}(\dot{z}_{si} - \dot{z}_{wi}) + k_{si}(z_{si} - z_{wi}) + k_{ti}(z_{ri} - z_{wi}) \quad (5)$$

For the system in hand, the second order LPF equations are:

$$\ddot{u}_i' + 2\varsigma\omega_c\dot{u}_i' + \omega_c^2 u_i' = \omega^2 u_i \quad (6)$$
$$\ddot{u}_i'' + 2\varsigma\omega_c\dot{u}_i'' + \omega_c^2 u_i'' = \omega^2 u_i' \quad (7)$$

with

$$\begin{aligned} u_i'' &= z_{bi} - z_{si} \\ z_{b1} &= z + a\theta + b\phi \\ z_{b2} &= z + a\theta - b\phi \\ z_{b3} &= z - a\theta + b\phi \\ z_{b4} &= z - a\theta - b\phi \end{aligned} \quad (8)$$

B. LQR ALGORITHM

The purpose of this section is to reduce the change in posture angles of FWLR in unstructured terrain, therefore, the θ and φ shown in Eq. (9) are set as the state variables, and the control input, disturbance vector, and system state equations are shown in Eqs. (10-12), respectively. The performance indexes of posture control are provided in Eqs. (13-14), and the Riccati equation and the control input (u) that minimizes J_1 and J_2 are depicted in Eqs. (15-16).

The state vector is given by

$$\begin{aligned} x = [&\dot{z}\dot{\theta}\dot{\phi}z\theta\phi\ \dot{z}_{s1}\dot{z}_{s2}\ \dot{z}_{s3}\dot{z}_{s4}\ z_{s1}z_{s2}z_{s3}z_{s4}\dot{z}_{w1}\ \dot{z}_{w2}\dot{z}_{w3} \\ &\dot{z}_{w4}z_{w1}z_{w2}z_{w3}z_{w4}\ \dot{u}_1'\dot{u}_2'\dot{u}_3'\dot{u}_4'u_1'u_2'u_3'u_4']^T \end{aligned} \quad (9)$$

The control input is given by

$$u = [\,u_1\ \ u_2\ \ u_3\ \ u_4\,] \quad (10)$$

The disturbance vectors is given by

$$w = [\,z_{r1}\ \ z_{r2}\ \ z_{r3}\ \ z_{r4}\,] \quad (11)$$

The state equation is given by

$$\dot{x} = A_d x + B_d u + D_d w \quad (12)$$

The performance indexes of posture control, $i = (1\sim4)$ is given by

$$\begin{aligned} J_1 = {} & \rho_1(\ddot{z})^2 + \rho_2(\Delta_{ti})^2 + \rho_3(\Delta_{bi})^2 + \rho_4(\Delta_{pd})^2 \\ & + \rho_5(\Delta_{ai})^2 + \rho_6(\Delta_{pp})^2 + \rho_7(z)^2 \end{aligned} \quad (13)$$
$$\begin{aligned} J_2 = {} & \rho_1(\ddot{z})^2 + \rho_2(\Delta_{ti})^2 + \rho_3(\Delta_{bi})^2 + \rho_4(\Delta_{d})^2 \\ & + \rho_5(\Delta_{ai})^2 + \rho_6(\Delta_{p})^2 + \rho_7(z)^2 \end{aligned} \quad (14)$$

The Reccati equation is given by

$$PA_d + A_d^T P - PB_d R^{-1} B_d^T P + Q = 0 \quad (15)$$

The control input u that minimizes J_1 and J_2 is given by

$$u = -kx = -R^{-1}B_d^T P x \quad (16)$$

among which, in the performance indexes, ρ_1, ρ_2, ρ_3, ρ_4, ρ_5, ρ_6, and ρ_7 are weighting factors. The tyre deflections, $_{ti}$, suspension deflections, $_{bi}$, integral of posture angles, $_{d}$, $_{pd}$, control input, $_{ai}$, and posture angles, $_{p}$, $_{pp}$ are given in Eqs. (17-23), respectively.

$$\begin{aligned} (\Delta_{ti})^2 = {} & (z_{w1} - z_{r1})^2 + (z_{w2} - z_{r2})^2 + (z_{w3} - z_{r3})^2 \\ & + (z_{w4} - z_{r4})^2 \end{aligned} \quad (17)$$
$$\begin{aligned} (\Delta_{bi})^2 = {} & (z_{w1} - z_{b1})^2 + (z_{w2} - z_{b2})^2 + (z_{w3} - z_{b3})^2 \\ & + (z_{w4} - z_{b4})^2 \end{aligned} \quad (18)$$
$$(\Delta_d)^2 = (\theta)^2 \quad (19)$$
$$(\Delta_{ai})^2 = (u_1)^2 + (u_2)^2 + (u_3)^2 + (u_4)^2 \quad (20)$$
$$(\Delta_p)^2 = (\phi)^2 \quad (21)$$
$$(\Delta_{pd})^2 = (\theta + 0.026)^2 \quad (22)$$
$$(\Delta_{pp})^2 = (\phi - 0.04)^2 \quad (23)$$

Because the LQR algorithm needs disturbance information from the terrain, and it can be estimated by the posture angles fed back by the gyroscope on the body. **Figs. 5(a)** shows the flow chart of terrain estimation, and Eqs. (24-25) represent the proposed terrain model, as long as the posture angles of FWLR are fed back, the terrain can be estimated.

$$z_{r1} = a\theta + b\phi$$

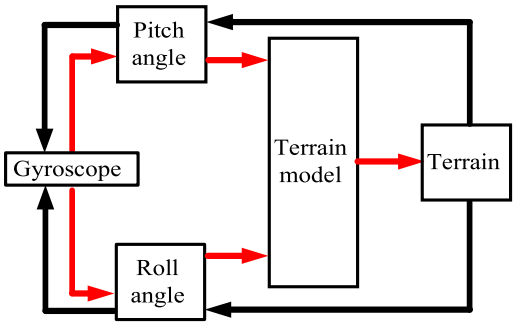

(a) Flow chart of terrain estimation

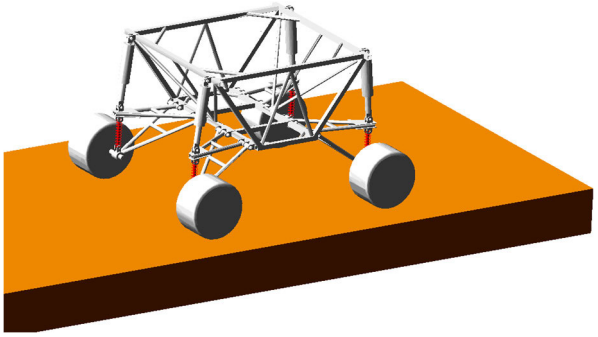

(b) Physical model in ADAMS

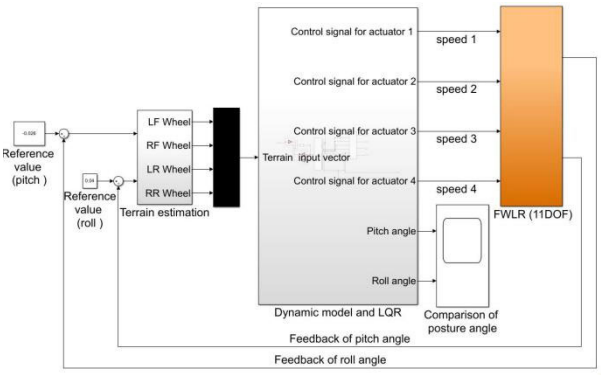

(c) Simulation model in MATLAB

FIGURE 5. Co-simulation of posture tracking.

$$z_{r2} = a\theta - b\phi$$
$$z_{r3} = -a\theta + b\phi$$
$$z_{r4} = -a\theta - b\phi \tag{24}$$

$$\begin{bmatrix} z_{r1} \\ z_{r2} \\ z_{r3} \\ z_{r4} \end{bmatrix} = \begin{bmatrix} a & b \\ a & -b \\ -a & b \\ -a & -b \end{bmatrix} \begin{bmatrix} \theta \\ \phi \end{bmatrix} \tag{25}$$

C. CO-SIMULATION AND EXPERIMENT

1) POSTURE TRACKING

To validate the validity of the proposed model and algorithm, posture tracking of FWLR with the co-simulation of ADAMS and MATLAB is carried out. The control principle is that the robot adjusts its posture according to the desired posture angles.

In the simulation, the two target values are set as $\theta = -0.026$ and $\varphi = 0.040$, the performance index is J_1, and the weighting factors shown in J_1 are $\rho_1 = 1$, $\rho_2 = 10^{-2}$, $\rho_3 = 10^{-2}$, $\rho_4 = 10^{5}$, $\rho_5 = 10^{-9}$, $\rho_6 = 10^{4.5}$, and $\rho_7 = 1$, the co-simulation is shown in **Figs. 5(b)** and **5(c)**. The simulation results are compared with the experimental results below.

To realize the comparison of the simulation and experiment of posture tracking, a control loop shown in **Figs. 6(a)** is built, and the corresponding controller depicted in **Figs. 6(b)** is designed. The Kvaser controller in this article is implemented on a PC in the MATLAB environment via the communication mode of the controller area network (CAN). All the investigated parameters can be measured and displayed in MATLAB, the controller mainly includes four modules:

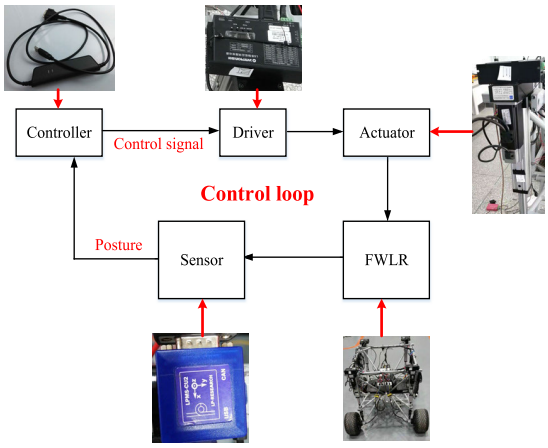

(a) Control loop

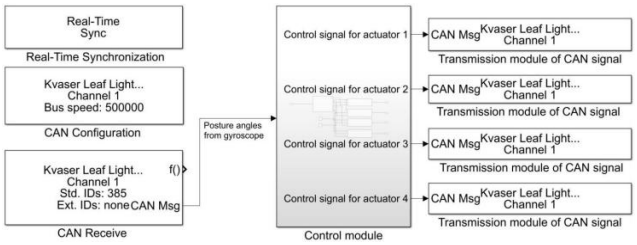

(b) Controller design

FIGURE 6. Posture tracking in experiment.

1) CAN Configuration. The communication mode of the control system is CAN, and this module is used to set the baud rate of CAN. In this article, the baud rate is 500K.
2) CAN Receive. This module is used to receive posture angles fed back by the gyroscope.
3) Control module. This module includes the dynamic model, terrain estimation model and LQR algorithm.
4) Transmission module of CAN signal. This module is used to transmit control signals to actuators.

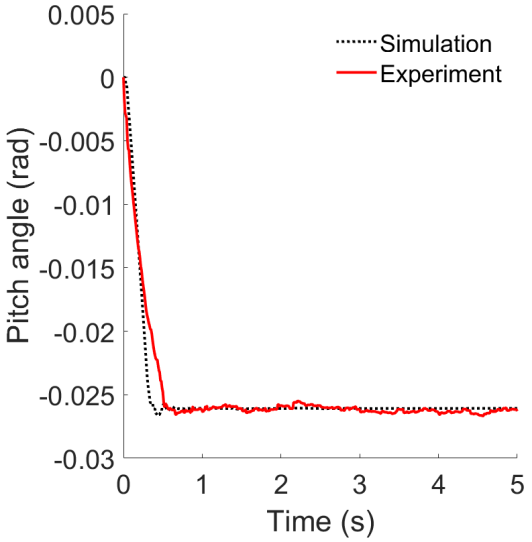

(a) Pitch angle

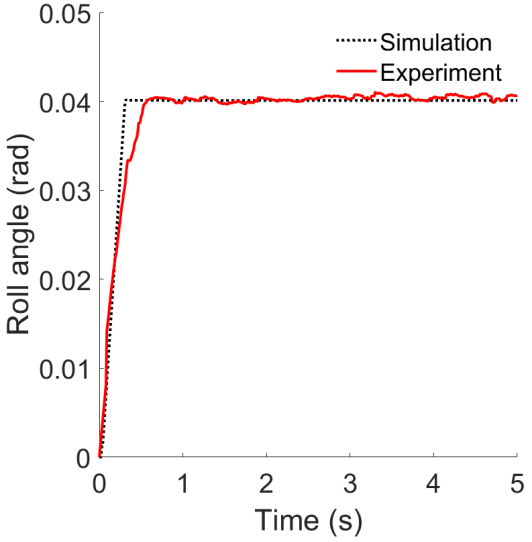

(b) Roll angle

FIGURE 7. Comparison of posture tracking.

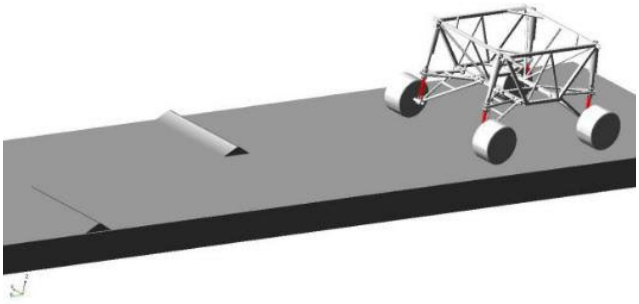

(a) Virtual unstructured terrain

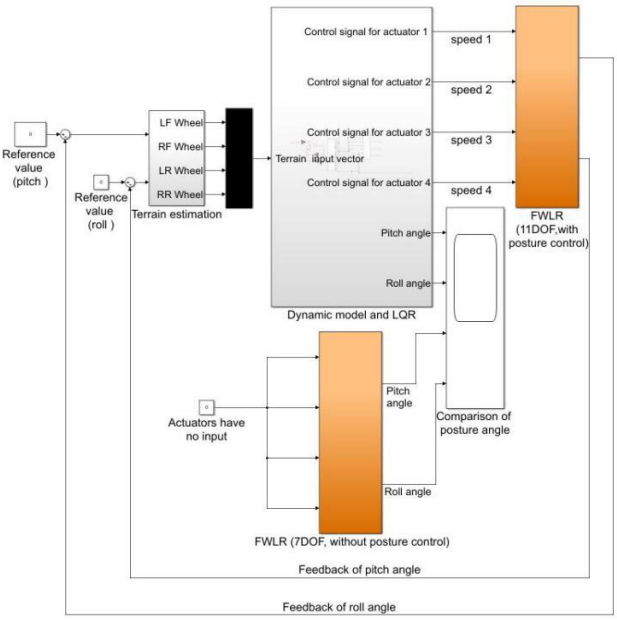

(b) Comparison of posture control in unstructured terrain

FIGURE 8. Co-simulation of posture control in unstructured terrain.

The parameter values in the experiment are the same as those in the co-simulation. In the experiment of posture tracking, the sampling rate of all sensors, devices and measurement system is 0.001s, the speed of FWLR is 0m/s, and the desired posture is $\theta = -0.026$, $\varphi = 0.040$. The experimental principle is that the desired posture is input into the control system firstly. The control signals are then sent to the corresponding actuator, and the posture of FWLR is adjusted by the output of actuators. Finally, the posture angles are fed back by the gyroscope installed in FWLR, and the angles will be compared with the desired angles until the posture tracking is achieved.

The comparison between the simulation and experiment of posture tracking is shown in **Fig 7**. The results illustrate that the steady-state values are consistent with the desired values, the steady-state time is approximately 0.5s, and the overshoot is very small. Generally, the validity of the model and algorithm is validated by the simulation and experiment. In addition, the simulation can achieve the steady state faster than the experiment, because there are errors in the experiment, and the main errors are as follows:

1) White noise of gyroscope.
2) Measurement and machining error. For example, it is difficult to achieve the moment of inertia of the robot accurately, but it has a great influence on the posture angles of the robot.

2) POSTURE CONTROL IN UNSTRUCTURED TERRAIN

The posture tracking of FWLR is validated by co-simulation and experiment, however, it is carried out under the condition that the robot does not move. To further validate the posture control ability of FWLR, a driving system and unstructured terrains are developed for FWLR, with purpose of testing the posture control performance of FWLR in unstructured terrain. In this subsection, the co-simulation and experiment of posture control in unstructured terrain are studied.

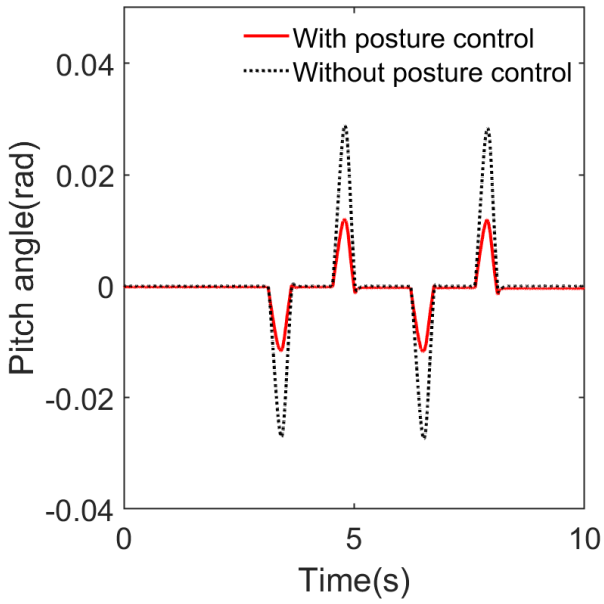

(a) Pitch angle

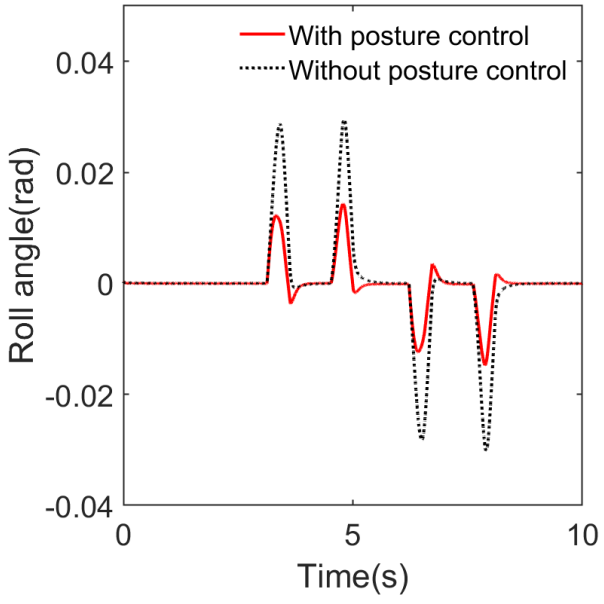

(b) Roll angle

FIGURE 9. Co-simulation results in unstructured terrain.

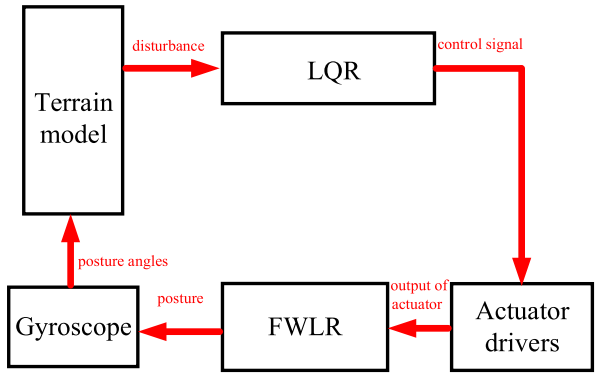

(a) Flow chart of posture control

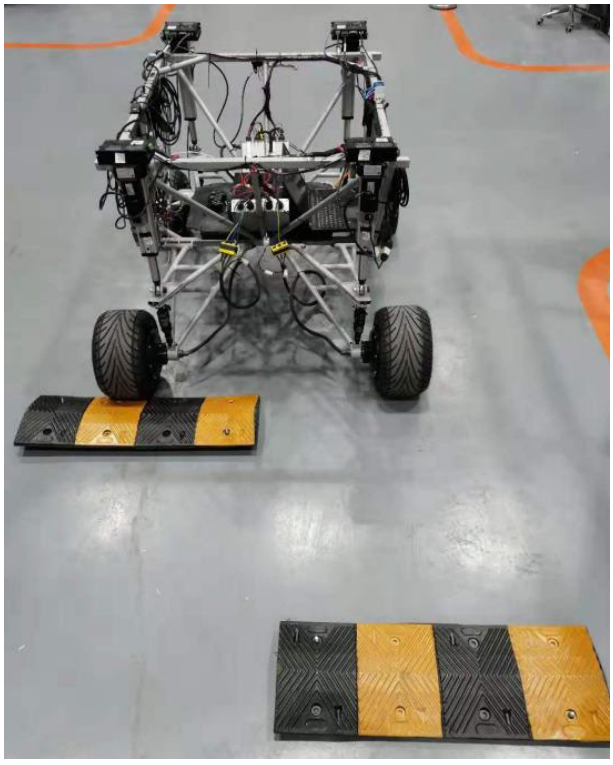

(b) unstructured terrain

FIGURE 10. Experiment of posture control in unstructured terrain.

The co-simulation of ADAMS and MATLAB with the comparison of posture control is carried out, and the simulation principle is as follows. Firstly, the posture angles in unstructured terrain are measured by the gyroscope. Secondly, the terrain information is estimated according to the angles, and the corresponding control signals are sent to the corresponding actuators. Finally, the posture control of FWLR in unstructured terrain is achieved as the adjustment of actuators. The virtual unstructured terrain built in ADAMS is shown in **Figs. 8(a)**, and the co-simulation model built in MATLAB is shown in **Figs. 8(b)**.

In the simulation, the speed of FWLR is 1m/s, the performance index is J_2, and the comparison of posture control is presented in **Fig. 9** and **Tab. 2.** The results showed that the model and algorithm proposed in this article can improve the posture control ability of FWLR in unstructured terrain, in which the improvement proportion of the pitch angle is 58.2%, the roll angle is 51.1%, and the average improvement is 54.65%.

To further verify the correctness of posture control of FWLR in unstructured terrain, an experiment is carried out based on the simulation. The controller used in the experiment is basically the same as that shown in **Fig. 6**, but the difference between them is that the performance index is J_2 shown in Eq (14). In the experiment, the sampling rate of all sensors, devices and measurement system is 0.001s, the speed of FWLR is 1m/s, and the desired posture is $\theta = 0$, $\varphi = 0$.

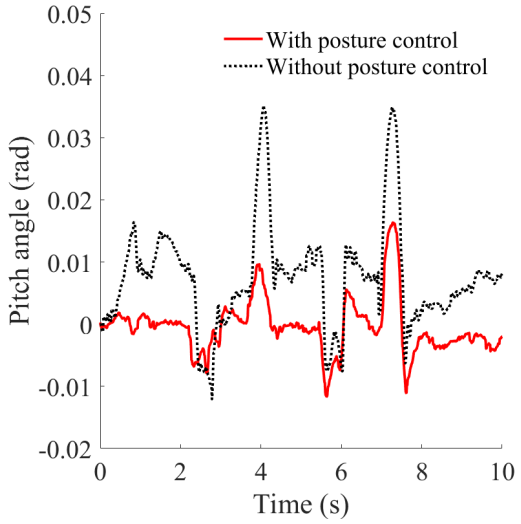

(a) Pitch angle

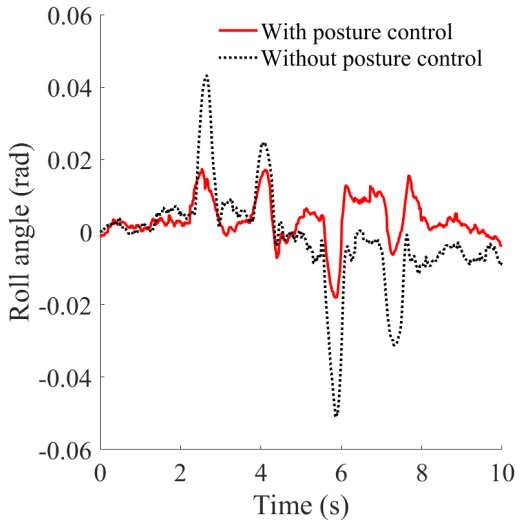

(b) Roll angle

FIGURE 11. Experimental results in unstructured terrain.

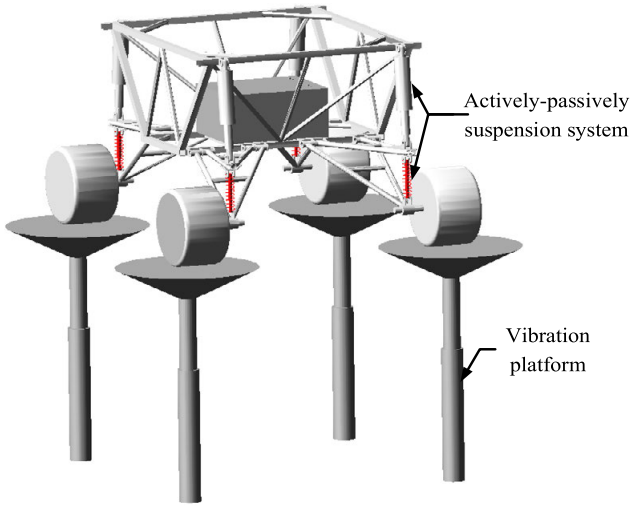

FIGURE 12. Vibration platform built in ADAMS.

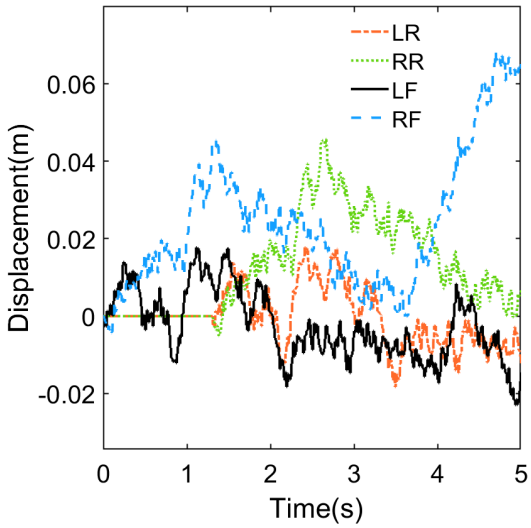

FIGURE 13. Random terrain output by vibration platform.

The obstacle size of the terrain is 1m × 0.4m × 0.075m. The flow chart and unstructured terrain are depicted in **Figs. 10(a)** and **10(b)**, respectively, and the experimental results are shown in **Fig. 11** and **Tab. 2**. The results show that the model and algorithm proposed in this article can obviously improve the performance of posture control in unstructured terrain, in which the improvement proportion of the pitch angle is 54%, the roll angle is 64%, and the average improvement is 59%. In addition, the experimental results and simulation results are basically the same, and the main errors in the experiment are as follows:

1) The moment of inertia of the robot is difficult to measure accurately.
2) The terrain model is linearized, which leads to errors between the estimated terrain and the actual terrain.
3) The maximum working speed of the actuator is 125mm/s, which limits the response of the control system.

TABLE 2. Comparison of posture control between simulation and experiment.

Posture / Comparison	Simulation		Experiment	
	Pitch	Roll	Pitch	Roll
With posture control	0.01206 rad	0.01476 rad	0.0163 rad	0.0181 rad
Without posture control	0.02884 rad	0.03017 rad	0.0352 rad	0.0511 rad
Improvement	58.2%	51.1%	54%	64%
Average improvement	54.65%		59%	

3) FREQUENCY RESPONSE FOR RANDOM ROADS

To verify the posture control performance of FWLR in different terrain, the frequency response in random terrain is analyzed with the co-simulation of ADAMS and MATLAB. In the simulation, the vibration platform is built in ADAMS, and the random terrain is input by a vibration platform.

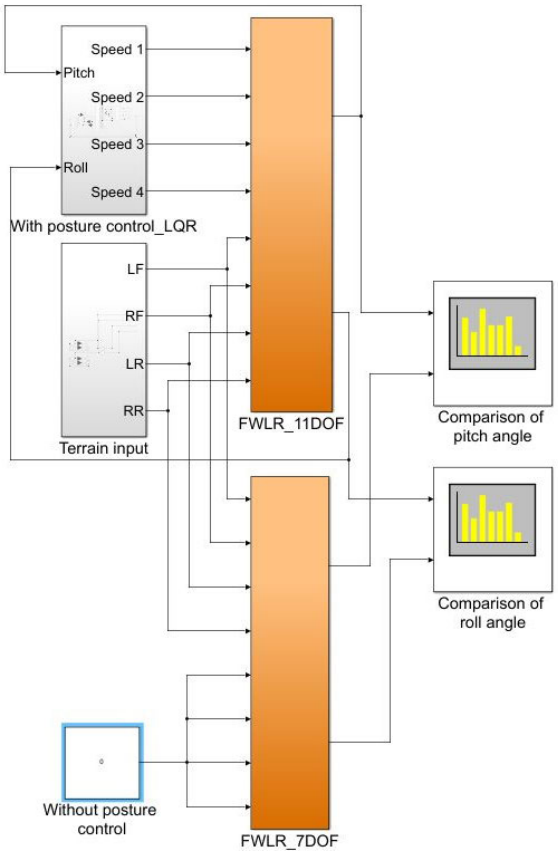

FIGURE 14. Co-simulation model of frequency response.

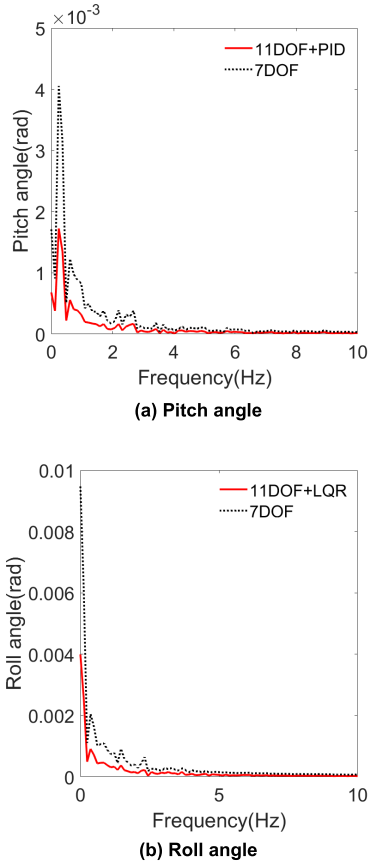

FIGURE 15. Results of frequency response.

The random terrain is obtained by Eq. (26) (shown in Fig. 13), and the parameter settings are depicted in [43], [44].

$$\begin{aligned} \dot{z}_j(t) &= -2\pi f_0 z_j(t) + 2\pi\sqrt{G_0 v} w_i(t) \\ z_{LF}(t) &= z_{LR}(t - 2a/v) \\ z_{RF}(t) &= z_{RR}(t - 2a/v) \end{aligned} \tag{26}$$

where $z_j(t)$ represents the input of the vibration platform to each wheel, $j = (LF, RF, LR, RR)$. $w_i(t)$ represents the input of random white noise, $i = (1 \sim 4)$. f_0 represents the lower cut-off frequency, $f_0 = 0.01$Hz. G_0 represents the road roughness coefficient, $G_0 = 5 \times 10^{-6}(\mathrm{m}^3/\mathrm{cycle})$. v represents the speed of FWLR, $v = 1$m/s.

The co-simulation model of frequency response is built in Fig. 14, and the comparison of posture angles is shown in Fig. 15. The results show that the pitch angle is reduced by more than 60%, and the roll angle is reduced by more than 50% within 5Hz. This shows that the proposed LQR controller can effectively improve the posture control performance of FWLR in low-frequency unstructured terrain. On the other hand, the following two reasons can also explain the validity of the frequency response.

1) The actively-passively suspension proposed in this article is a series slow active suspension, which is suitable for posture control of low-frequency unstructured terrain within 6Hz.
2) In addition, the LPF shown in Eqs. (6-7) is included in the posture control model, this means that the posture control can be achieved in low-frequency terrain.

Overall, the novel suspension and LQR controller proposed in this article can improve the posture control performance FWLR in low frequency unstructured terrain.

IV. PERFORMANCE OF RIDE COMFORT (VIBRATION ISOLATION PERFORMANCE)

Posture control and ride comfort are two key factors that affect the off-road performance of the robot in unstructured terrain. The posture control of FWLR is realized by the proposed suspension system, control model, and algorithm in this article. In this subsection, the influence of the actively-passively suspension system on the ride comfort of the robot is studied, and the pitch angular acceleration and roll angular acceleration are regarded as two evaluation indexes of ride comfort [45].

A. INFLUENCE OF ACTIVE SYSTEM (POSTURE CONTROL) ON RIDE COMFORT

To validate the influence of the posture control on the ride comfort of FWLR, the flow chart and co-simulation model are presented in **Figs. 16(a)** and **16(b)**, respectively. The values of the parameters in the simulation are the same as those shown in subsection III, and the speed is also 1m/s.

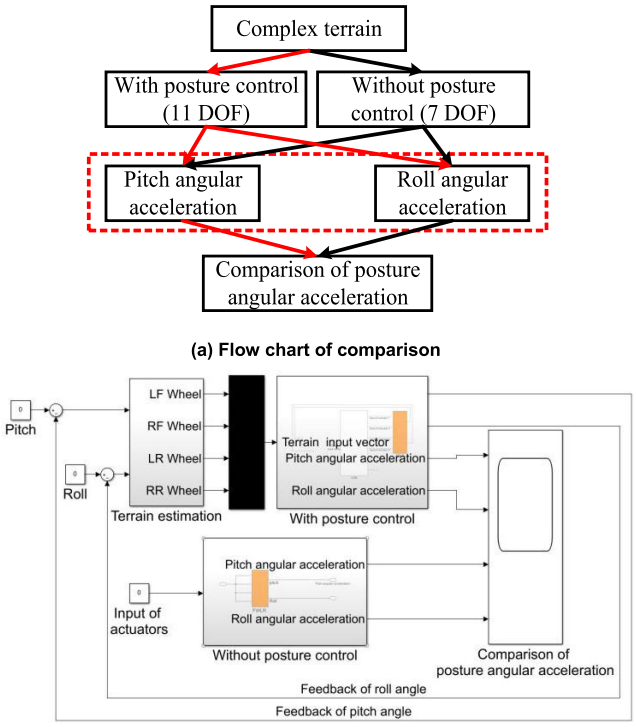

(a) Flow chart of comparison

(b) Co-simulation model of posture angular acceleration in MATLAB

FIGURE 16. Comparison of posture angular acceleration in unstructured terrain.

TABLE 3. Comparison of posture angular acceleration.

Posture angular acceleration / Comparison	Pitch	Roll
With posture control	4.465 rad/s^2	4.645 rad/s^2
Without posture control	5.002 rad/s^2	5.873 rad/s^2
Improvement	20.91%	10.74%
Average improvement	15.83%	

The comparison is shown in **Fig. 17.** The results show that the pitch angular acceleration and the roll angular acceleration are reduced obviously with the posture control, and the specific results are presented in **Tab. 3**. In conclusion, the posture angular acceleration is reduced by 15.83% on average, which enhances the vibration isolation performance of FWLR.

B. INFLUENCE OF PASSIVE SYSTEM (SPRING-DAMPING)ON RIDE COMFORT

In this subsection, the influence of the passive system on ride comfort is studied, because the passive system is part of the proposed actively-passively suspension, and the vibration isolation system is rarely used in traditional robots. In the simulation, the posture cannot be changed, so the 7 DOF and 3 DOF dynamic model shown in **Figs. 18(a)** and **18(b)**, respectively, can be used to compare the influence of the passive system on ride comfort **[46], [47]**, and the corresponding equations are shown in Eqs. (27-35). The 7 DOF

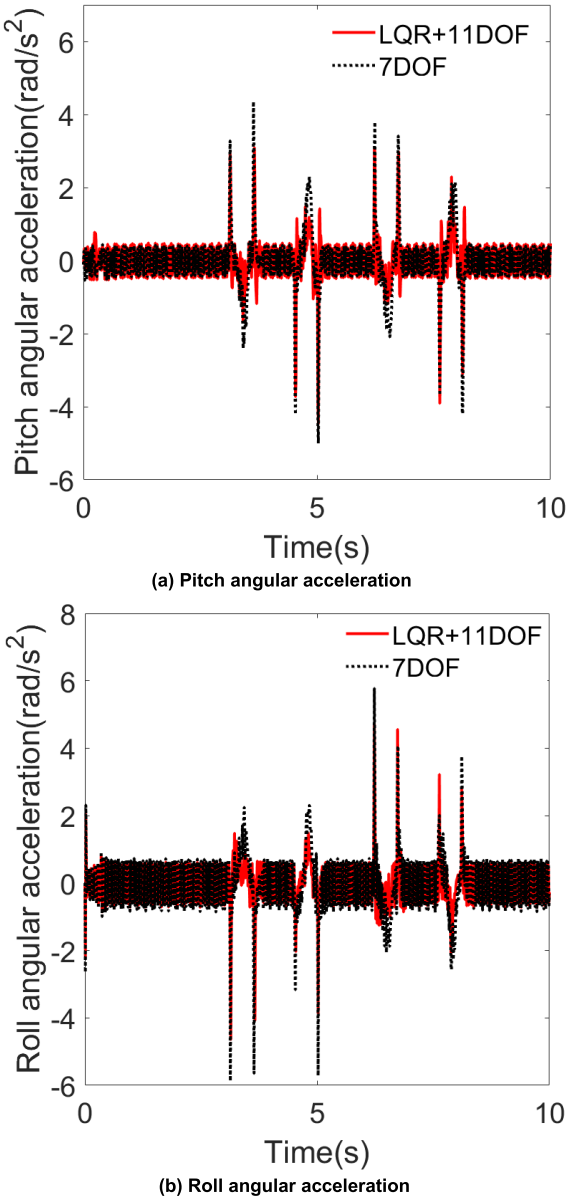

(a) Pitch angular acceleration

(b) Roll angular acceleration

FIGURE 17. Results of posture angular acceleration in unstructured terrain.

model represents the robot with the spring-damping system that is regarded as an elastic component, and the 3 DOF model represents the robot with the spring-damping system that is regarded as a rigid body. In the simulation, the ramp terrain is input to each tyre, the slope of the terrain is 1, −1,1 and −1, respectively, and the interval time of input is 1s.

The flow chart and simulation model are presented in **Figs. 19(a)** and **19(b)**, respectively, and the results are shown in **Figs. 20(a)** and **20(b)**. The results illustrate that the posture angular acceleration is significantly reduced by 46.7% on average, which means the passive system of the proposed suspension can effectively improve the ride comfort of FWLR in unstructured terrain. These findings occur because the ground impact is absorbed by the passive system, and the

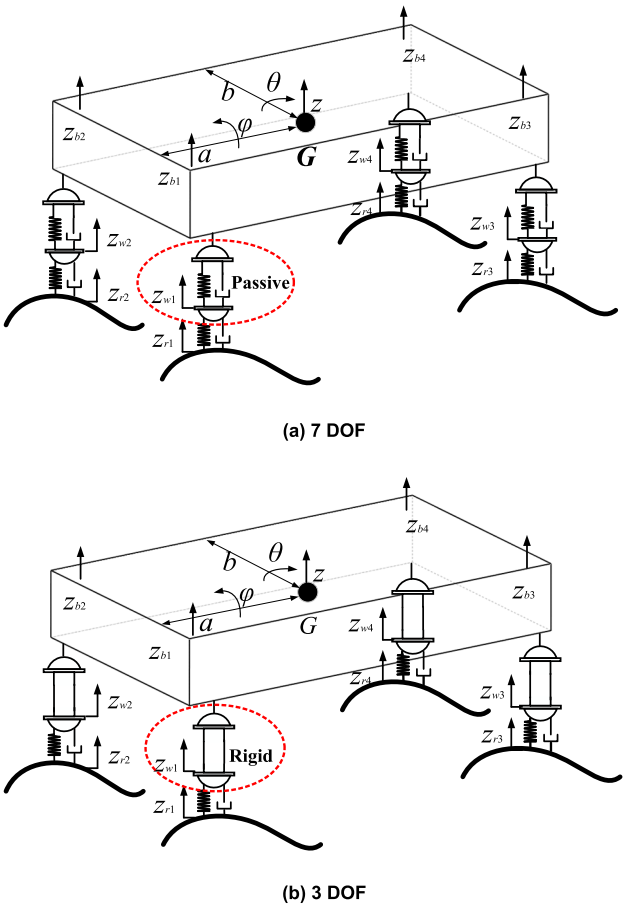

(a) 7 DOF

(b) 3 DOF

FIGURE 18. Dynamic model with different DOF.

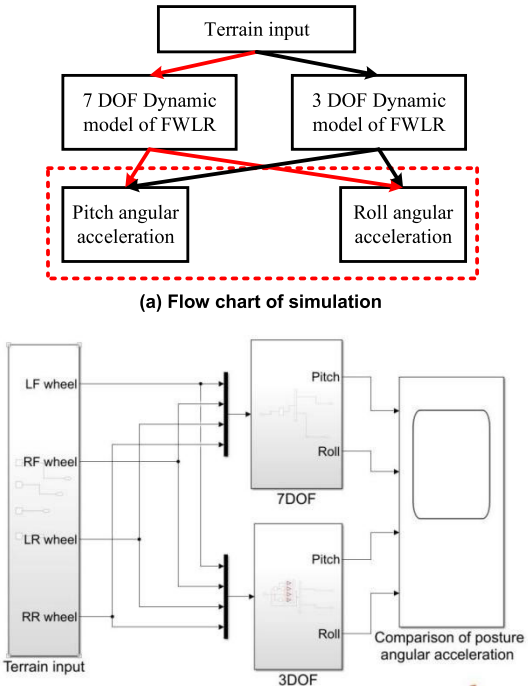

(a) Flow chart of simulation

(b) Simulation model in MATLAB

FIGURE 19. Comparison of ride comfort.

impact energy is dissipated into the air in the form of thermal energy.

Overall, both the active system and passive system of the suspension proposed in this article can improve the ride comfort of the robot in unstructured terrain.

1) 7 DOF MODEL

The equations of the vertical motion of the tyres, $i = (1\sim4)$ is given by

$$m_{wi}\ddot{z}_{wi} = c_{si}(\dot{z}_{bi} - \dot{z}_{wi}) + k_{si}(z_{bi} - z_{wi}) + k_{ti}(z_{ri} - z_{wi}) \quad (27)$$

The equation of the vertical motion of the body is given by

$$\begin{aligned} m\ddot{z} = {} & c_{s1}(\dot{z}_{w1} - \dot{z}_{b1}) + k_{s1}(z_{w1} - z_{b1}) + c_{s2}(\dot{z}_{w2} - \dot{z}_{b2}) \\ & + k_{s2}(z_{w2} - z_{b2}) + c_{s3}(\dot{z}_{w3} - \dot{z}_{b3}) + k_{s3}(z_{w3} - z_{b3}) \\ & + c_{s4}(\dot{z}_{w4} - \dot{z}_{b4}) + k_{s4}(z_{w4} - z_{b4}) \end{aligned} \quad (28)$$

The equation of the pitch motion of the body is given by

$$\begin{aligned} I_p\ddot{\theta} = {} & -a[c_{s3}(\dot{z}_{w3} - \dot{z}_{b3}) + k_{s3}(z_{w3} - z_{b3}) + c_{s4}(\dot{z}_{w4} - \dot{z}_{b4}) \\ & + k_{s4}(z_{w4} - z_{b4})] + a[c_{s1}(\dot{z}_{w1} - \dot{z}_{b1}) + k_{s1}(z_{w1} - z_{b1}) \\ & + c_{s2}(\dot{z}_{w2} - \dot{z}_{b2}) + k_{s2}(z_{w2} - z_{b2})] \end{aligned} \quad (29)$$

The equation of the roll motion of the body is given by

$$\begin{aligned} I_r\ddot{\phi} = {} & [c_{s1}(\dot{z}_{w1} - \dot{z}_{b1}) + k_{s1}(z_{w1} - z_{b1}) - c_{s2}(\dot{z}_{w2} - \dot{z}_{b2}) \\ & - k_{s2}(z_{w2} - z_{b2})]b + [c_{s3}(\dot{z}_{w3} - \dot{z}_{b3}) + k_{s3}(z_{w3} - z_{b3}) \\ & - c_{s4}(\dot{z}_{w4} - \dot{z}_{b4}) - k_{s4}(z_{w4} - z_{b4})]b \end{aligned} \quad (30)$$

The matrix expression of 7 DOF is given by

$$M\ddot{X} + C\dot{X} + KX = K_tZ_r + C_t\dot{Z}_r \quad (31)$$

2) 3 DOF MODEL

The equation of vertical motion of the body is given by

$$\begin{aligned} m\ddot{z} = {} & c_{t1}(\dot{z}_{r1} - \dot{z}_{b1}) + k_{t1}(z_{r1} - z_{b1}) + c_{t2}(\dot{z}_{r2} - \dot{z}_{b2}) \\ & + k_{t2}(z_{r2} - z_{b2}) + c_{t3}(\dot{z}_{r3} - \dot{z}_{b3}) + k_{t3}(z_{r3} - z_{b3}) \\ & + c_{t4}(\dot{z}_{r4} - \dot{z}_{b4}) + k_{t4}(z_{r4} - z_{b4}) \end{aligned} \quad (32)$$

The equation of the pitch motion of the body is given by

$$\begin{aligned} I_p\ddot{\theta} = {} & a[c_{r1}(\dot{z}_{r1} - \dot{z}_{b1}) + k_{t1}(z_{r1} - z_{b1}) + c_{t2}(\dot{z}_{r2} - \dot{z}_{b2}) \\ & + k_{t2}(z_{r2} - z_{b2})] - a[c_{t3}(\dot{z}_{r3} - \dot{z}_{b3}) + k_{t3}(z_{r3} - z_{b3}) \\ & + c_{t4}(\dot{z}_{r4} - \dot{z}_{b4}) + k_{t4}(z_{r4} - z_{b4})] \end{aligned} \quad (33)$$

The equation of the roll motion of the body is given by

$$\begin{aligned} I_r\ddot{\phi} = {} & b[c_{t1}(\dot{z}_{r1} - \dot{z}_{b1}) + k_{t1}(z_{r1} - z_{b1}) + c_{t3}(\dot{z}_{r3} - \dot{z}_{b3}) \\ & + k_{t3}(z_{r3} - z_{b3})] - b[c_{t2}(\dot{z}_{r2} - \dot{z}_{b2}) + k_{t2}(z_{r2} - z_{b2}) \\ & + c_{t4}(\dot{z}_{r4} - \dot{z}_{b4}) + k_{t4}(z_{r4} - z_{b4})] \end{aligned} \quad (34)$$

The matrix expression of 3 DOF is given by

$$M^*\ddot{X} + C^*\dot{X} + K^*X = K_t^*Z_r + C_t^*\dot{Z}_r \quad (35)$$

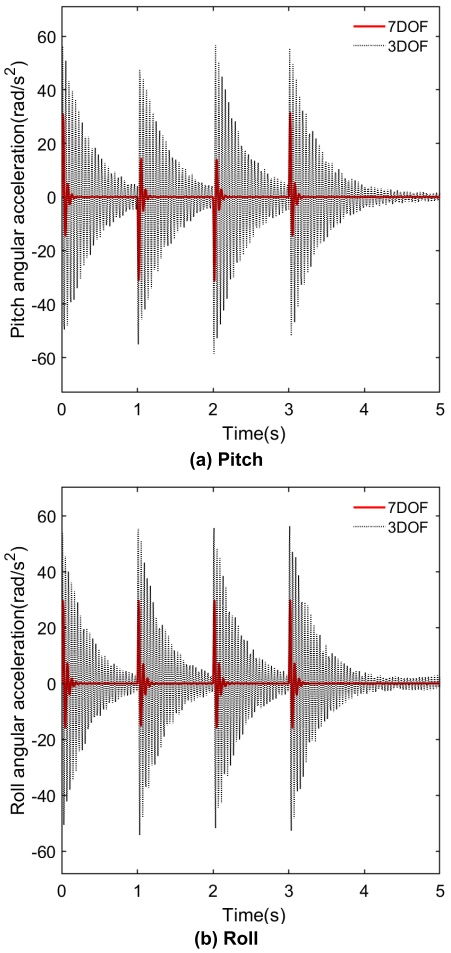

FIGURE 20. Comparison of posture angular acceleration in ramp terrain.

V. CONCLUSION

This article for the first time proposed and developed a novel reconfigurable hybrid wheel-legged mobile robot. The posture control and ride comfort of FWLR in unstructured terrain can be achieved by the actively-passively suspension system of each leg at the same time. The suspension system is composed of an actuator and spring-damping system, respectively, and they are connected in series. In addition, the design concept of FWLR is universal, it can be used for the design of other types of robots and vehicles

The closed-loop and decoupled dynamic model of posture control is formulated, with which the LQR controller with SLPF is proposed. The simulation and experimental results show that the posture angles in unstructured terrain are significantly reduced by more than 50%. On the other hand, the frequency response is analyzed, the results present that the posture angles are reduced by more than 50% in low-frequency unstructured terrain. In addition, the ride comfort performance of FWLR is validated by different dynamic models proposed in this article, the results indicate that both the posture control and passive system of FWLR can improve the ride comfort by more than 15% and 40%. Overall, the novel wheel-legged robot, control model and algorithm proposed in this article can improve the problems of posture control and ride comfort of traditional robots.

The research of this article has positive reference significance and potential practical value for developing the mechanism design and promoting the engineering application of wheel-legged robots. The future work of this research is to realize automatic driving and keep balanced posture in unstructured terrain by equipping with environment sensing system.

APPENDICES

See table 4.

$$M = \begin{bmatrix} m & 0 & 0 & 0 & 0 & 0 & 0 \\ 0 & I_p & 0 & 0 & 0 & 0 & 0 \\ 0 & 0 & I_r & 0 & 0 & 0 & 0 \\ 0 & 0 & 0 & m_{w1} & 0 & 0 & 0 \\ 0 & 0 & 0 & 0 & m_{w2} & 0 & 0 \\ 0 & 0 & 0 & 0 & 0 & m_{w3} & 0 \\ 0 & 0 & 0 & 0 & 0 & 0 & m_{w4} \end{bmatrix}$$

$$K_t = \begin{bmatrix} 0 & 0 & 0 & 0 \\ 0 & 0 & 0 & 0 \\ 0 & 0 & 0 & 0 \\ k_t & 0 & 0 & 0 \\ 0 & k_t & 0 & 0 \\ 0 & 0 & k_t & 0 \\ 0 & 0 & 0 & k_t \end{bmatrix}$$

$$C = \begin{bmatrix} 4c_s & 0 & 0 & -c_s & -c_s & -c_s & -c_s \\ 0 & 4a^2c_s & 0 & -ac_s & -ac_s & ac_s & ac_s \\ 0 & 0 & 4b^2c_s & -bc_s & bc_s & -bc_s & bc_s \\ -c_s & -ac_s & -bc_s & c_s + c_t & 0 & 0 & 0 \\ -c_s & -ac_s & bc_s & 0 & c_s + c_t & 0 & 0 \\ -c_s & ac_s & -bc_s & 0 & 0 & c_s + c_t & 0 \\ -c_s & ac_s & bc_s & 0 & 0 & 0 & c_s + c_t \end{bmatrix}$$

$$K = \begin{bmatrix} 4k_s & 0 & 0 & -k_s & -k_s & -k_s & -k_s \\ 0 & 4a^2k_s & 0 & -ak_s & -ak_s & ak_s & ak_s \\ 0 & 0 & 4b^2k_s & -bk_s & bk_s & -bk_s & bk_s \\ -k_s & -ak_s & -bk_s & k_s + k_t & 0 & 0 & 0 \\ -k_s & -ak_s & bk_s & 0 & k_s + k_t & 0 & 0 \\ -k_s & ak_s & -bk_s & 0 & 0 & k_s + k_t & 0 \\ -k_s & ak_s & bk_s & 0 & 0 & 0 & k_s + k_t \end{bmatrix}$$

$$C_t = \begin{bmatrix} 0 & 0 & 0 & 0 \\ 0 & 0 & 0 & 0 \\ 0 & 0 & 0 & 0 \\ c_t & 0 & 0 & 0 \\ 0 & c_t & 0 & 0 \\ 0 & 0 & c_t & 0 \\ 0 & 0 & 0 & c_t \end{bmatrix}$$

TABLE 4. Parameters list.

m_t: tyre mass, (kg)	m_s: link mass, (kg)	m: body mass, (kg)	z_r: terrain input, (m)
z_w: vertical displacement of tyre, (m)	z_r: vertical excitation of terrain, (m)	z: vertical displacement of body, (m)	c_s: damper damping (N*s/m)
k_s: spring stiffness, (N/m)	c_t: tyre damping (N*s/m)	k_t: tyre stiffness, (N/m)	z_{wi}: vertical displacement of tyre, (m), i=1, 2, 3, 4
z_{bi}: vertical displacement of four corners, i=1, 2, 3, 4, (m)	F_i: force of actuator, i=1,2,3,4, (N)	z_{si}: vertical displacement of link, i=1, 2, 3, 4, (m)	z_{ri}: vertical excitation of terrain, (m), i=1, 2, 3, 4
θ: pitch angle, (rad)	φ: roll angle, (rad)	a: 1/2 wheelbase, (m)	b: 1/2 wheelbase, (m)
J_1: performance index of posture tracking	J_2: performance index of posture control in unstructured terrain	ς : damping ratio	ω_c : filter cut-off frequency, (Hz)
ς : damping ratio	z_s: vertical displacement of link, (m)	ω : circular frequency, (rad/s)	u : control input vector
u_i : actuator control demand signal, i=1, 2, 3, 4	$u_i^{'}$: second-order filtered control demand signal, i=1, 2, 3, 4	$u_i^{''}$: fourth-order filtered control demand signal, i=1, 2, 3, 4	w : terrain input vector
$I\theta$: integral of pitch angle, (rad)	$I\varphi$: integral of roll angle, (rad)	ρ_i: weighting factors, i=1, 2, ,3, 4, 5, 6, 7	M*: mass matrix of 3 DOF
C*: damping matrix of 3 DOF	K*: stiffness matrix of 3 DOF	K_t*: tyre stiffness matrix of 3 DOF	C_t*: tyre damping matrix of 3 DOF
M: mass matrix of 7 DOF	C: damping matrix of 7 DOF	K: stiffness matrix of 7 DOF	K_t: tyre stiffness matrix of 7 DOF
C_t: tyre damping matrix of 7 DOF	A_d: system matrix	B_d: input matrix of feedback	D_d: input matrix

$$M^* = \begin{bmatrix} m & 0 & 0 \\ 0 & I_p & 0 \\ 0 & 0 & I_r \end{bmatrix} C^* = \begin{bmatrix} 4c_t & 0 & 0 \\ 0 & 4a^2c_t & 0 \\ 0 & 0 & 4b^2c_t \end{bmatrix}$$

$$K^* = \begin{bmatrix} 4k_t & 0 & 0 \\ 0 & 4a^2k_t & 0 \\ 0 & 0 & 4b^2k_t \end{bmatrix} K_t^* = \begin{bmatrix} k_t & k_t & k_t & k_t \\ ak_t & ak_t & -ak_t & -ak_t \\ bk_t & -bk_t & bk_t & -bk_t \end{bmatrix}$$

$$C_t^* = \begin{bmatrix} c_t & c_t & c_t & c_t \\ ac_t & ac_t & -ac_t & -ac_t \\ bc_t & -bc_t & bc_t & -bc_t \end{bmatrix}$$

REFERENCES

[1] H. Jiang, G. Xu, W. Zeng, and F. Gao, "Design and kinematic modeling of a passively-actively transformable mobile robot," *Mechanism Mach. Theory*, vol. 142, Dec. 2019, Art. no. 103591.

[2] J. Niu, H. Wang, H. Shi, N. Pop, D. Li, S. Li, and S. Wu, "Study on structural modeling and kinematics analysis of a novel wheel-legged rescue robot," *Int. J. Adv. Robot. Syst.*, vol. 15, no. 1, pp. 1–17, Jan. 2018.

[3] K. Nagatani, A. Yamasaki, K. Yoshida, and T. Adachi, "Development and control method of six-wheel robot with rocker structure," in *Proc. IEEE Int. Workshop Saf., Secur. Rescue Robot.*, Rome, Italy, Sep. 2007, p. 189.

[4] M. Tarokh and G. J. McDermott, "Kinematics modeling and analyses of articulated rovers," *IEEE Trans. Robot.*, vol. 21, no. 4, pp. 539–553, Aug. 2005.

[5] A. Bouloubasis, G. McKee, and P. Tolson, "Novel concepts for a planetary surface exploration rover," *Ind. Robot, Int. J.*, vol. 34, no. 2, pp. 116–121, Mar. 2007.

[6] H. R. Fernandes and A. P. Garcia, "Design and control of an active suspension system for unmanned agricultural vehicles for field operations," *Biosyst. Eng.*, vol. 174, pp. 107–114, Oct. 2018.

[7] M. M. Gor, P. M. Pathak, A. K. Samantaray, J.-M. Yang, and S. W. Kwak, "Fault accommodation in compliant quadruped robot through a moving appendage mechanism," *Mechanism Mach. Theory*, vol. 121, pp. 228–244, Mar. 2018.

[8] A. Laurenzi, E. M. Hoffman, M. P. Polverini, and N. G. Tsagarakis, "An augmented kinematic model for the Cartesian control of the hybrid wheeled-legged quadrupedal robot CENTAURO," *IEEE Robot. Autom. Lett.*, vol. 5, no. 2, pp. 508–515, Apr. 2020.

[9] D. Kim, H. Hong, H. S. Kim, and J. Kim, "Optimal design and kinetic analysis of a stair-climbing mobile robot with rocker-bogie mechanism," *Mechanism Mach. Theory*, vol. 50, pp. 90–108, Apr. 2012.

[10] D. Choi, Y. Kim, S. Jung, H. S. Kim, and J. Kim, "Improvement of step-climbing capability of a new mobile robot RHyMo via kineto-static analysis," *Mechanism Mach. Theory*, vol. 114, pp. 20–37, Aug. 2017.

[11] F. Ma, L. Ni, and L. Wu, "Pitching posture closed loop control of wheel-legged all terrain mobile robot with active suspension," *Trans. Chin. Soc. Agricult. Eng.*, vol. 34, no. 20, pp. 20–27, 2018.

[12] E. Garcia, J. C. Arevalo, G. Muñoz, and P. Gonzalez-de-Santos, "Combining series elastic actuation and magneto-rheological damping for the control of agile locomotion," *Robot. Auton. Syst.*, vol. 59, no. 10, pp. 827–839, Oct. 2011.

[13] Q. Wei, M. Luo, J. Zhao, and F. Guo, "Trajectory planning and control for hopping robot at the stance phase," in *Proc. IEEE Int. Conf. Mechatronics Automat. (ICMA)*, Takamatsu, Japan, Aug. 2017, pp. 1608–1613.

[14] G. He and Z. Geng, "Dynamics synthesis and control for a hopping robot with articulated leg," *Mechanism Mach. Theory*, vol. 46, no. 11, pp. 1669–1688, Nov. 2011.

[15] F. Cordes, A. Dettmann, and F. Kirchner, "Locomotion modes for a hybrid wheeled-leg planetary rover," in *Proc. IEEE Int. Conf. Robot. Biomimetics*, Karon Beach, Thailand, Dec. 2011, pp. 2586–2592.

[16] K. D. Iagnemma, A. Rzepniewski, S. Dubowsky, P. Pirjanian, T. L. Huntsberger, and P. S. Schenker, "Mobile robot kinematic reconfigurability for rough terrain," *Proc. SPIE*, vol. 4196, pp. 413–420, Oct. 2000.

[17] D. Wettergreen, S. Moreland, K. Skonieczny, D. Jonak, D. Kohanbash, and J. Teza, "Design and field experimentation of a prototype lunar prospector," *Int. J. Robot. Res.*, vol. 29, no. 12, pp. 1550–1564, Oct. 2010.

[18] B. H. Wilcox, T. Litwin, J. Biesiadecki, J. Matthews, M. Heverly, J. Morrison, J. Townsend, N. Ahmad, A. Sirota, and B. Cooper, "Athlete: A cargo handling and manipulation robot for the moon," *J. Field Robot.*, vol. 24, no. 5, pp. 421–434, May 2007.

[19] T. Aoki, Y. Murayama, and S. Hirose, "Development of a transformable three-wheeled lunar rover: Tri-star IV," *J. Field Robot.*, vol. 31, no. 1, pp. 206–223, Jan. 2014.
[20] A. Halme, I. Leppänen, S. Salmi, and S. Ylönen, "Hybrid locomotion of a wheel-legged machine," in *Proc. 3rd Int. Conf. Climbing Walking Robots (CLAWAR)*, Madrid, Spain, Oct. 2000, pp. 1–7.
[21] W. Reid, F. J. Perez-Grau, A. H. Goktogan, and S. Sukkarieh, "Actively articulated suspension for a wheel-on-leg rover operating on a martian analog surface," in *Proc. IEEE Int. Conf. Robot. Automat. (ICRA)*, Stockholm, Sweden, May 2016, pp. 5596–5602.
[22] Y. Luo, Q. Li, and Z. Liu, "Design and optimization of wheel-legged robot: Rolling-wolf," *Chin. J. Mech. Eng.*, vol. 27, no. 6, pp. 1133–1142, 2014.
[23] C. Grand, F. Benamar, F. Plumet, and P. Bidaud, "Stability and traction optimization of a reconfigurable wheel-legged robot," *Int. J. Robot. Res.*, vol. 23, nos. 10–11, pp. 1041–1058, Oct. 2004.
[24] C. Grand, F. Benamar, and F. Plumet, "Motion kinematics analysis of wheeled–legged rover over 3D surface with posture adaptation," *Mechanism Mach. Theory*, vol. 45, no. 3, pp. 477–495, Mar. 2010.
[25] S. Bazeille, V. Barasuol, M. Focchi, I. Havoutis, M. Frigerio, J. Buchli, D. G. Caldwell, and C. Semini, "Quadruped robot trotting over irregular terrain assisted by stereo-vision," *Intell. Service Robot.*, vol. 7, no. 2, pp. 67–77, Apr. 2014.
[26] X. Pan, K. Xu, and W. Yao, "Design and analysis of a wheel-legged robot with a suspension system," *Robot*, vol. 40, no. 3, pp. 1–12, 2018.
[27] R. Siegwart, P. Lamon, T. Estier, M. Lauria, and R. Piguet, "Innovative design for wheeled locomotion in rough terrain," *Robot. Auton. Syst.*, vol. 40, nos. 2–3, pp. 151–162, Aug. 2002.
[28] T. Thomson, I. Sharf, and B. Beckman, "Kinematic control and posture optimization of a redundantly actuated quadruped robot," in *Proc. IEEE Int. Conf. Robot. Automat.*, Saint Paul, MN, USA, May 2012, pp. 1895–1900.
[29] Y. Sun and S. Ma, "Decoupled kinematic control of terrestrial locomotion for an ePaddle-based reconfigurable amphibious robot," in *Proc. IEEE Int. Conf. Robot. Automat. (ICRA)*, Shanghai, China, May 2011, pp. 1223–1228.
[30] S. Nakajima, E. Nakano, and T. Takahashi, "Motion control technique for practical use of a leg-wheel robot on unknown outdoor rough terrains," in *Proc. IEEE/RSJ Int. Conf. Intell. Robots Syst. (IROS)*, Sendai, Japan, Sep./Oct. 2004, pp. 1353–1358.
[31] J. Xie, R. C. Wang, Q. M. Ye, P. Xiang, and L. Chen, "Study on coordination control of body posture for active suspension with linear motor," *Chin. J. Automot. Eng.*, vol. 5, no. 5, pp. 341–347, 2015.
[32] X. B. Zhu and F. Gao, "Simulation and analysis on semi-active control technology of multi-axle vehicle suspension," *Trans. Chin. Soc. Agricult. Mach.*, vol. 39, no. 8, pp. 33–37 and 61, 2008.
[33] L. Zheng, Y. N. Li, J. S. Wei, and J. Shao, "Coordinated control of semi-active suspension with magnetorheological dampers and electrical power assist steer system," *J. Vib. Eng.*, vol. 22, no. 5, pp. 503–511, 2009
[34] H. Pan and W. Sun, "Nonlinear output feedback finite-time control for vehicle active suspension systems," *IEEE Trans. Ind. Informat.*, vol. 15, no. 4, pp. 2073–2082, Apr. 2019.
[35] H. Pan, X. Jing, W. Sun, and H. Gao, "A bioinspired dynamics-based adaptive tracking control for nonlinear suspension systems," *IEEE Trans. Control Syst. Technol.*, vol. 26, no. 3, pp. 903–914, May 2018.
[36] H. Pan, H. Li, W. Sun, and Z. Wang, "Adaptive fault-tolerant compensation control and its application to nonlinear suspension systems," *IEEE Trans. Syst., Man, Cybern. Syst.*, vol. 50, no. 5, pp. 1766–1776, May 2020.
[37] A. Tharakeshwar and A. Ghosal, "Modeling and simulation of a three-wheeled mobile robot on uneven terrains with two-degree-of-freedom suspension mechanisms," *Mech. Based Des. Struct. Mach.*, vol. 43, no. 4, pp. 466–486, Oct. 2015.
[38] G. Chen, B. Jin, and Y. Chen, "Tripod gait-based turning gait of a six-legged walking robot," *J. Mech. Sci. Technol.*, vol. 31, no. 3, pp. 1401–1411, Mar. 2017.
[39] G. Chen, B. Jin, and Y. Chen, "Accurate position and posture control of a redundant hexapod robot," *Arabian J. Sci. Eng.*, vol. 42, no. 5, pp. 2031–2042, May 2017.
[40] Q. Li, H. Ren, W. Pu, and J. Jiang, "Trotting gait control of the quadruped robot with an elastic linkage," *Robot*, vol. 41, no. 2, pp. 1–9, 2019.
[41] Y. Li, B. Li, and X. Rong, "Mechanical design and gait planning of a hydraulically actuated quadruped bionic robot," *J. Shandong Univ., Eng. Sci.*, vol. 41, no. 5, pp. 32–36, 2011.
[42] C. Semini, N. G. Tsagarakis, E. Guglielmino, M. Focchi, F. Cannella, and D. G. Caldwell, "Design of HyQ—A hydraulically and electrically actuated quadruped robot," *Proc. Inst. Mech. Eng. I, J. Syst. Control Eng.*, vol. 225, no. 6, pp. 831–849, 2011.
[43] S. M. Lou, Z. Fu, and C. S. Xu, "Design and simulation of a sliding mode controller for vehicle semi-active suspension," *Automot. Eng.*, vol. 32, no. 8, pp. 719–726, 2010.
[44] D. Grabowski, M. Szczodrak, and A. Czyzewski, "Economical methods for measuring road surface roughness," *Metrol. Meas. Syst.*, vol. 25, no. 3, pp. 533–549, 2018.
[45] C. Gu, J. Yin, and X. Chen, "Robust control and optimization of a rocker-pushrod electromagnetic active suspension," *Automot. Eng.*, vol. 40, no. 1, pp. 34–40, 2018.
[46] I. Youn, L. Wu, E. Youn, and M. Tomizuka, "Attitude motion control of the active suspension system with tracking controller," *Int. J. Automot. Technol.*, vol. 16, no. 4, pp. 593–601, Aug. 2015.
[47] L. Wu, I. Youn, and M. Tomizuka, "Integrated posture motion and lateral stability control of a vehicle via active suspension and rear-wheel steering control system," *Dyn. Vehicles Roads Tracks*, pp. 365–374, 2016.

LIWEI NI received the M.S. degree from the Henan University of Science and Technology, in 2015. He is currently pursuing the Ph.D. degree with the College of Automotive Engineering, Jilin University. His research interests include wheel-legged robot and all-terrain vehicle.

FANGWU MA received the B.S. and M.S. degrees in automotive engineering from Jilin University, in 1982 and 1988, respectively, and the Ph.D. degree from the Imperial College London, in 1999. His research interests include wheel-legged robot, all-terrain vehicle, intelligent vehicle, and lightweight design. He is an SAE Fellow and the VP of FISITA.

LIANG WU received the M.S. and Ph.D. degrees from Gyeongsang National University, in 2010 and 2015, respectively. His research interests include wheel-legged robot and all-terrain vehicle.